J. Am. Soc. Mass Spectrom. (2016) 27:319–328
DOI: 10.1007/s13361-015-1277-9

RESEARCH ARTICLE

Mechanistic Study on Electronic Excitation Dissociation of the Cellobiose-Na^+ Complex

Yiqun Huang,[1,2] Yi Pu,[1,3] Xiang Yu,[1,2] Catherine E. Costello,[1,2,3] Cheng Lin[1,2]

[1]Mass Spectrometry Resource, Boston University School of Medicine, Boston, MA 02118, USA
[2]Department of Biochemistry, Boston University School of Medicine, Boston, MA 02118, USA
[3]Department of Chemistry, Boston University, Boston, MA 02215, USA

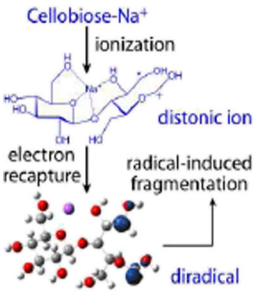

Abstract. The recent development of electron activated dissociation (ExD) techniques has opened the door for high-throughput, detailed glycan structural elucidation. Among them, ExD methods employing higher-energy electrons offer several advantages over low-energy electron capture dissociation (ECD), owing to their applicability towards chromophore-labeled glycans and singly charged ions, and ability to provide more extensive structural information. However, a lack of understanding of these processes has hindered rational optimization of the experimental conditions for more efficient fragmentation as well as the development of informatics tools for interpretation of the complex glycan ExD spectra. Here, cellobiose-Na^+ was used as the model system to investigate the fragmentation behavior of metal-adducted glycans under irradiation of electrons with energy exceeding their ionization potential, and served as the basis on which a novel electronic excitation dissociation (EED) mechanism was proposed. It was found that ionization of the glycan produces a mixture of radical cations and ring-opened distonic ions. These distonic ions then capture a low-energy electron to produce diradicals with trivial singlet-triplet splitting, and subsequently undergo radical-induced dissociation to produce a variety of fragment ions, the abundances of which are influenced by the stability of the distonic ions from which they originate.

Keywords: Electronic excitation dissociation (EED), FTICR, Oligosaccharides, Fragmentation mechanism, Molecular dynamics simulation, Density functional theory, Tandem mass spectrometry

Received: 17 June 2015/Revised: 2 September 2015/Accepted: 5 September 2015/Published Online: 2 October 2015

Introduction

The utility of ion/electron interactions in ion structural elucidation was first demonstrated with the development of a technique known as the electron impact excitation of ions from organics (EIEIO), whereby inelastic ion/electron scattering leads to ion activation and dissociation [1]. However, it is the discovery of electron capture dissociation (ECD) that catapulted the use of electrons for tandem mass spectrometry (MS/MS) analysis into the limelight [2]. In ECD, a low-energy electron is captured by a multiply charged analyte ion, generating a charge-reduced species that subsequently undergoes radical-driven fragmentations. For peptide ions, ECD is capable of producing extensive backbone N–C_α bond cleavages, while leaving the labile side-chain modifications intact. For this reason, ECD, along with its sibling, electron transfer dissociation (ETD) [3], has quickly become a popular alternative to the slow-heating tandem MS methods, such as collisionally activated dissociation (CAD) and infrared multiphoton dissociation (IRMPD), and these methods are now widely used in proteomics studies, especially for characterization of post-translational modifications [4–6].

Because the electron capture cross-section drops sharply at higher electron energies, ECD is generally performed with irradiation of low-energy electrons (<0.2 eV). After the initial definition of the technique, it was later discovered that a second, broad local maximum exists at an electron energy around 10 eV, which results from dissociative recombination into electronically excited states [7]. The fragmentation process following capture of a "hot" electron is termed hot-ECD, or HECD, and is believed to proceed via a mechanism similar to ECD. A unique property of HECD is its tendency to induce

Electronic supplementary material The online version of this article (doi:10.1007/s13361-015-1277-9) contains supplementary material, which is available to authorized users.

Correspondence to: Cheng Lin; *e-mail:* chenglin@bu.edu

more extensive secondary fragmentation, and this has been utilized for differentiation of isomeric residues. Irradiation of peptide ions by electrons with energy greater than 10 eV may further ionize the precursor ion, which then undergoes intramolecular charge and hydrogen atom transfers and captures a slow electron to induce fragmentation. This process is termed electronic excitation dissociation (EED) because it involves an electronically excited precursor ion formed upon electron capture by the charge-increased species [8, 9]. EED should not be confused with another tandem MS technique known as the electron ionization dissociation (EID) [10]. In EID, electrons with an energy greater than 30 eV have been utilized to induce successive ionizations of peptide ions, and the subsequent electron capture by the doubly ionized precursor ion forms a hydrogen-deficient radical cation to produce ECD-like fragments. An advantage of EED and EID is their applicability towards singly charged ions that cannot be analyzed by ECD because of its charge-reducing nature.

Despite their analytical potentials, EED and other electron activated dissociation (ExD) methods employing higher-energy electrons have initially garnered far less interest than ECD because of their lower fragmentation efficiencies. Further, ECD and ETD had been found to work so well for protein characterization that there seemed to be little incentive for developing other ExD methods. However, it soon became clear that some biomolecules cannot be effectively analyzed by ECD or ETD as both demand a multiply charged cationic precursor in order to generate at least one charged product. A major driving force for the development of ExD methods beyond ECD is the characterization of glycans. In particular, glycosaminoglycans (GAGs), a class of linear glycans with various degrees of sulfation, are best analyzed in their anionic form to minimize uninformative, proton-mediated SO_3 losses. Electron detachment dissociation (EDD) and negative ETD (NETD) have been shown to be highly effective for structural analysis of GAGs and sialylated glycans since they drive multiply deprotonated precursor ions to undergo charge reduction via electron detachment or reverse electron transfer and thereby initiate radical-induced fragmentation with high degree of sulfate retention [11–14].

Structural characterization of other classes of glycans, including *N*-linked and *O*-linked glycans, presents a different analytical challenge. Unlike linear biopolymers such as proteins and GAGs, these glycans can assume varied two-dimensional topologies that differ in branching patterns and/or linkage configurations. Reliable linkage determination often hinges upon the observation of specific cross-ring fragments, but they are frequently missing in CAD and IRMPD spectra. Although ECD and ETD can provide considerably more structural information than CAD [15–18], they too have limitations. Besides their inapplicability to singly charged precursors, their rather unsatisfactory performance with alkali metal-adducts (especially for permethylated glycans) and their tendency to generate uninformative tag loss for chromophore-labeled glycans, could compromise their utility in on-line LC-MS/MS analyses. Further, even ECD and ETD may not always produce sufficient cross-ring fragment(s) needed for exhaustive isomer differentiation [17, 19, 20]. Fortunately, all these limitations can be overcome by using electrons of higher energies as demonstrated by several research groups [16, 19–21].

In 2003, Zubarev et al. reported that oligosaccharide cations with one or more charges could undergo extensive fragmentation when irradiated by electrons with energy exceeding their ionization potential [21]. At that time, such fragmentation was believed to be caused by electron impact vibrational excitation, and given the name electron-induced dissociation, or EID. The authors noted that the EID fragmentation pattern of a glycan often resembled that of ECD, and acknowledged that EID did not usually produce more cross-ring cleavages than CAD. These seemingly underwhelming results may be in part due to the innocent choice of instrument parameters that were not optimum for this class of compounds, as revealed later [20]. O'Connor et al. showed that irradiation of doubly charged sodiated and permethylated glycans with 5–14 eV electrons could produce fragmentation complementary to CAD, possibly by the hot-ECD process [16]. Håkansson et al. discovered that addition of a fluorescent tag led to richer EID product ion spectra, and attributed this effect to electronic excitation facilitated by the aromatic tag [22]. Electronic excitation was also invoked by Amster et al. to explain the similarity between the EID and EDD spectra of GAG anions [23]. It now seems clear that several distinct ion activation and dissociation processes can take place when a glycan cation is irradiated by high-energy electrons, including hot-ECD, EED, and EIEIO. Although the generic term of electron-induced dissociation is often used to describe these processes, it does not adequately reflect the nature of their differences, and further adds confusion by sharing the same acronym, EID, as electron ionization dissociation. The fact that singly charged glycan cations could produce radical fragments only by irradiation with electrons whose energy exceeds their ionization potential suggests an ionization-recapture mechanism similar to that proposed for EED of peptide ions [8]. Despite many references to electronic excitation, the details of the process remain murky. The recent demonstration of EED's potential for glycan structural elucidation illuminated the necessity for carrying out a theoretical investigation on the glycan EED mechanism. Insights into the EED process may lead to rational optimization of the experimental conditions, including the choice of charge carriers and the exploration of various derivatization schemes, to improve the fragmentation efficiency. Further, as shown in our previous studies, a sound mechanistic understanding of the fragmentation process is important for development of bioinformatics software for accurate interpretation of the tandem mass spectra [24].

Here, the EED fragmentation behavior of Na^+-adducted cellobiose, a disaccharide standard, was investigated theoretically to open the pathway for development of a general mechanism for EED of metal-bound glycans.

Experimental

Mass Spectrometry Analysis

HPLC-grade water and methanol were purchased from Fisher Scientific (Pittsburgh, PA, USA). All other chemicals were acquired from Sigma-Aldrich (St. Louis, MO, USA) and used as is. The reducing end ^{18}O-labeling was achieved by incubating cellobiose in $H_2{}^{18}O$ (97%) with 2-aminopyridine as the catalyst at 90°C overnight. The ^{18}O-labeled cellobiose was dissolved to a concentration of 5 μM in 50:50:1 water:methanol:formic acid solution containing 10–20 μM of sodium acetate. The sample was loaded into a pulled glass capillary with a 1 μm orifice and directly infused into the mass spectrometer.

All experiments were performed on a 12-T solariX hybrid Qh-Fourier transform ion cyclotron resonance (FTICR) mass spectrometer equipped with an indirectly heated cathode dispenser (Bruker Daltonics, Bremen, Germany). The quadrupole-isolated, singly charged Na^+-adducts were externally accumulated in the collision cell and transferred to the ICR cell. EED was performed with the cathode potential set between –10 and –16 V, and the cathode heating current at 1.5 A. The extraction lens bias was set to be approximately the same as the cathode potential to control the electron density inside the ICR cell. Typically, 20 transients were averaged to improve the *S/N* ratio. Typical mass accuracy with external calibration is around 2 ppm. Fragment ion assignment was performed manually with assistance from an in-house Python program.

Theoretical Modeling

The low-energy conformers of the cellobiose-Na^+ complex and their corresponding steric energies were explored by the molecular dynamics (MD) simulation, using the CHARMm force field, and utilizing a variety of initial geometries of cellobiose with different Na^+ binding sites. The initial geometry was successively optimized using the steepest descent and the conjugate gradient methodologies. Each preliminarily optimized structure was heated gradually from 50 to 700 K in 2000 1-fs long steps, followed by system equilibration at 700 K for 1 ps, and then subjected to MD trajectory calculation. Forty unequilibrated geometries were recorded at a time interval of 5 ps during each 200-ps trajectory run. Temperature-independent geometry optimization was performed on all collected geometries using the conjugate gradient algorithm. A cellobiose-Na^+ binding pattern was deemed typical if it could be reached via multiple trajectories with different initial geometries. The conformation space was then clustered based on the cellobiose-Na^+ binding patterns. All MD simulations were carried out using the standard dynamics cascade and minimization modules of the Discovery Studio 2.5.2 software (Accelrys, San Diego, CA, USA).

The mechanistic study was conducted using a procedure similar to that described in the previous publication [24]. Briefly, density functional theory (DFT)-based calculations were performed to determine the energetically favored conformers of the cellobiose-Na^+ complex and the dissociative potential energy surfaces. The relative stability of the most stable conformers with different Na^+ binding patterns was estimated at the B3LYP/6-31+G(d,p)//B3LYP/6-31G(d) level of theory. The full potential energy surfaces were investigated at the B3LYP/6-31G(d) level. When necessary, augmented basis sets were also utilized to calculate single point energies at certain reaction steps as described in the Results and Discussion section. The B3LYP/6-31G(d) electronic energy was corrected by the zero point vibrational energy with a scaling factor of 0.9806 [25], and used as the zero Kelvin enthalpy. The energetics of possible electronic excitations of the lowest energy conformer of the cellobiose-Na^+ complex were calculated using the time-dependent DFT (TDDFT) methodology, at the B3LYP/6-31G(d) level. All quantum mechanical calculations were performed using the Gaussian 03 or 09 program suite [26] at the Scientific Computing Facilities at Boston University.

Results and Discussion

Electronic Excitation Dissociation of the Cellobiose-Na^+ Complex

The 12 eV EED spectrum of the ^{18}O-labeled cellobiose-Na^+ complex is shown in Figure 1. The fragment ions were assigned using the Domon-Costello nomenclature [27]. The ^{18}O-labeling of the reducing-end not only allows differentiation of the non-reducing-end and reducing-end fragments, but also permits unambiguous identification of non-trivial cross-ring fragments at the reducing end. The term "trivial" is used here to describe cross-ring cleavages that produce uninformative neutral losses. For example, the 0,4- or 1,3-cleavage within the 1→4 linked reducing glucose ring would lead to loss of $C_2H_4O_2$ that can also result from the 0,4-, 1,3-, or 2,4-cleavage at the non-reducing glucose ring; thus the resultant fragment ions are simply labeled as M – $C_2H_4O_2$ in the spectrum. Besides neutral losses, EED of Na^+-bound cellobiose also generated an abundance of glycosidic and cross-ring fragments. The most abundant cross-ring fragments by far are the $^{3,5}A_2$ and $^{1,5}X_1$ ions, although other cross-ring fragments, including the $^{2,4}A_2$, $^{0,2}X_1$, $^{1,5}A_2$, $^{0,2}A_2$, and the isomeric $^{0,3}A_2$ and $^{1,4}A_2$ ions, were also produced. The $^{1,5}A_n$ and $^{1,5}X_n$ series can be produced from residues containing linkage(s) at any position; these products are thus structurally of little more use than those resulting from glycosidic cleavages, but the other cross-ring fragments provide valuable linkage information.

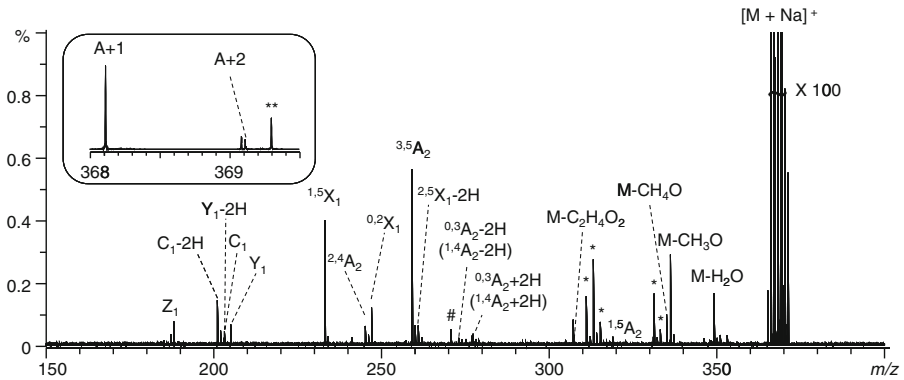

Figure 1. The EED spectrum of the cellobiose-Na^+ complex. # marks an electronic noise peak, * marks fragments generated from co-isolated unknown contaminant(s) due to their unusually large mass defects. The inset shows a zoomed-in view of the A+1 and A+2 isotopic peaks of the precursor ion, and ** marks a contaminant that could potentially give rise to fragment ions marked by *

The Binding Characteristics and the Conformation Space Clustering of the Cellobiose-Na^+ Complex

The most important parameters that describe the conformation of disaccharides are the extent of rotation of each monosaccharide residue about its respective glycosidic bond, as defined by the two dihedral angles: Φ (O5′-C1′-O4-C4 for cellobiose, Supporting Scheme S1) and Ψ (C1′-O4-C4-C5). Although the conformation space of native disaccharides may be explored systematically by grid search of the two dihedral angles [28–30], such systematic investigation cannot be performed on glycan-metal complexes because of the presence of noncovalent interactions. Instead, MD simulation was used here to explore the conformation space and to determine the typical Na^+-binding characteristics of the cellobiose-Na^+ system. DFT-based molecular modeling was then carried out on the lowest energy conformer found by the MD simulation to derive the EED mechanism.

The MD simulation revealed that the conformation space of the cellobiose-Na^+ complex can be divided into five sub-spaces based on the cellobiose-Na^+ binding pattern. For each cluster, the lowest-energy conformer was reoptimized using the density functional theory, and the optimized geometries are shown in Figure 2. The first major binding pattern is represented by structure **1a**, in which Na^+ interacts with four oxygen atoms: O6′, O5′, O4, and O3. The corresponding O-Na^+ distances are 2.30, 2.23, 2.96, and 2.24 Å, and the two dihedral angles Φ and Ψ are –82.7° and –100.6°, respectively. Both glucosyl rings are in the chair configuration, similar to the lowest energy conformer of the native cellobiose previously determined using the MM3 force field [29]. Structure **1b** represents the second major binding pattern, in which Na^+ interacts with O6′, O5′, O3′, O4, and O3, with the corresponding O-Na^+ distances being 2.37, 2.27, 2.35, 2.80, and 2.26 Å, respectively. The two dihedral angles Φ (–74.4°) and Ψ (–102.4°) are close in value to those in structure **1a**. Different from structure **1a**, the non-reducing

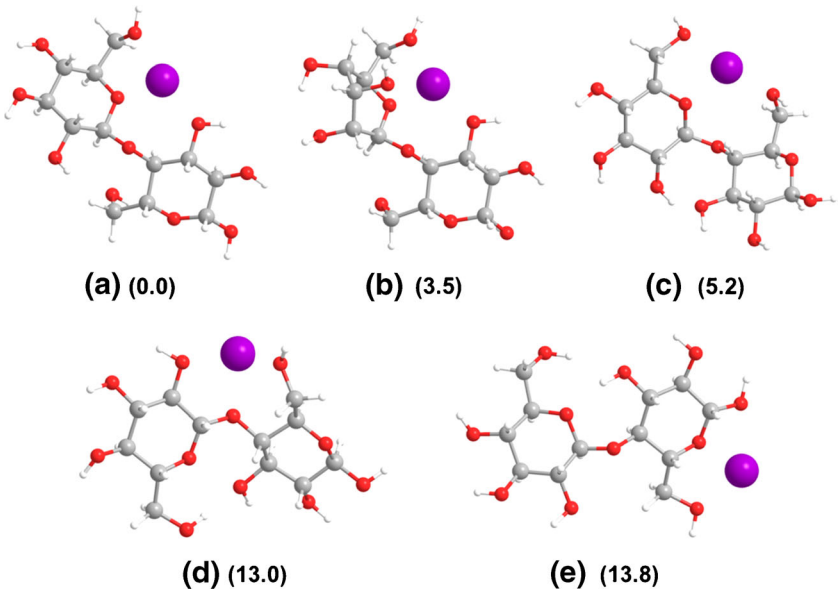

Figure 2. Typical low-energy conformers of the cellobiose-Na^+ complex. The number in parentheses indicates the potential energy (in kcal/mol) of each structure relative to structure **1a**

glucosyl ring in structure **1b** adopts the boat configuration to allow Na^+-O3′ interaction. In the cellobiose-Mg^{2+} system, such a structure was found to be the most stable as it led to stronger glycan-Mg^{2+} interaction and an overall decrease in potential energy despite the higher steric strain. However, in the cellobiose-Na^+ system, the electrostatic interaction between the metal cation and the glycan moiety is not as strong, and structure **1b** was found to be 3-4 kcal/mol higher in energy than **1a**. The third major binding pattern is represented by structure **1c**, which involves Na^+-binding to only three oxygen atoms, O6′, O5′, and O6, with the corresponding O-Na^+ distances being 2.23, 2.31, and 2.20 Å, respectively, and the two dihedral angles $\Phi = 65.2°$ and $\Psi = -148.8°$. In contrast to structures **1a** and **1b**, the glycosidic oxygen in **1c** no longer binds Na^+, while O6 from the more flexible C6 primary hydroxyl participates in the Na^+-glycan interaction. With both glucosyl rings in the chair configuration, steric strain is minimized in structure **1c**, at the price of reduced Na^+-glycan interaction. The last two typical binding patterns are represented by structures **1d** and **1e**, where both glucosyl rings are in the chair configuration. In structure **1d**, Na^+ binds to O2′, O6, and O4, at distances of 2.22, 2.34, and 2.23 Å, respectively, and $\Phi = -60.6°$ and $\Psi = -131.7°$. In structure **1e**, Na^+ binds to O6, O5, and O1, all from the reducing ring, at distances of 2.37, 2.18, 2.69Å, respectively, and $\Phi = -77.4°$ and $\Psi = -133.9°$. Conformers resembling structures **1d** and **1e** are much higher in energy and should not comprise an appreciable population.

The relative energies of structures **1a**–**1e** are listed in Figure 2. Since geometry optimization at the B3LYP/6-31+G(d,p) level coupled with normal frequency calculation was beyond our computational capability, the B3LYP/6-31+G(d,p) single point energy was calculated on the B3LYP/6-31G(d) geometry for all five structures to investigate the basis set augmentation effect. Full geometry optimization at the B3LYP/6-31+G(d,p) level without frequency calculation was also performed for structures **1a**, **1b**, and **1c** to evaluate the reliability of using the B3LYP/6-31+G(d,p)//B3LYP/6-31G(d) energies for estimating the relative stability. As shown in Table 1, the basis set augmentation does not change the stability order of typical cellobiose-Na^+ conformers and the B3LYP/6-31+G(d,p)//B3LYP/6-31G(d) treatment appears to be a valid cost-effective alternative to the full B3LYP/6-31+G(d,p) level optimization. Structure **1a** should be the predominant conformer at room temperature, and was therefore used in further theoretical modeling.

Table 1. The Relative Energy (kcal/mol) of the Conformers **1a**, **1b**, and **1c**, Calculated at the B3LYP/6-31+G(d,p)//B3LYP/6-31G(d) and the B3LYP/6-31+G(d,p) Levels of Theory

	1a	1b	1c
B3LYP/6-31+G(d,p)//B3LYP/6-31G(d)	0.0	3.5	4.7
Full B3LYP/6-31+G(d,p) level optimization	0.0	3.2	4.4

Electron-Induced Ionization

The calculated ionization energy of structure **1a** is 11.07 eV, around 1 eV lower than the electron energy used. The DFT calculation revealed that ionization of structure **1a** initially forms a radical cation, **2a**, with its spin density mainly localized at O5. The calculation also predicted the presence of two low-lying open-ring structures, **2b** and **2c**, formed by the cleavage of the C1–C2 or C1′–C2′ bond in **1a** during ionization, respectively (Scheme 1). At the B3LYP/6-31G(d) level with only the electronic energy taken into account, **2b** is 1.8 kcal/mol higher in energy than **2a**, and the energy barrier associated with the ring-opening process is 2.3 kcal/mol. Inclusion of the zero point vibrational energy increases the endothermicity of the ring-opening process to 2.6 kcal/mol but reduces the barrier to 2.2 kcal/mol. Single point energy was further calculated at the B3LYP/6-31+G(d,p), B3LYP/6-311++G(2d,p), and B3LYP/6-311++G(3df,2p) levels, on the B3LYP/6-31G(d) geometries of **2a**, **2b**, and the transition states. The electronic energies obtained at these levels were then corrected by the B3LYP/6-31G(d) level zero point vibrational energies, and the results are tabulated in Table 2. At the level with the largest basis set, structure **2b** becomes energetically preferred. Thus, the ring-opening process can occur spontaneously during ionization, even if **2a** is formed initially. Structure **2b** depicted in Scheme 1 can be regarded as a resonance-stabilized distonic ion with two canonical structures. The calculated spin density is 0.38 and 0.16 at C2 and O2, and 0.13, 0.17, and 0.09 at C1, O5, and O1, respectively. The canonical form with the radical at C2 and the positive charge at C1 is the preferred structure because it not only minimizes charge-charge repulsion due to the longer distance between the ionization site and Na^+ but also permits more extensive charge delocalization among C1 and its two neighboring oxygen atoms.

The second open-ring structure, **2c**, is 2.6 kcal/mol higher in energy than **2a**, if only the electronic energy is considered. This energy difference increases to 3.4 kcal/mol with inclusion of the zero point vibrational energy (Table 2). No tight transition state can be found for the conversion of **2a** to **2c** at the B3LYP/6-31G(d) level. With single point energies calculated using the more extensive 6-311+G(d,p), 6-311++G(2d,p), and 6-311++G(3df,2p) basis sets on the B3LYP/6-31G(d) geometries, the energy difference decreases to 3.4, 2.6, and 1.9 kcal/mol, respectively. By extrapolation, the energy gap between structures **2a** and **2c** could become even narrower as the basis set limit is approached. Like **2b**, structure **2c** can also be viewed as a two-structure, resonance-stabilized distonic ion (Scheme 1). In **2c**, the spin density is fairly evenly distributed among O5′, C1′, O4, C2′, and O2′, with values of 0.12, 0.26, 0.09, 0.18, and 0.21, respectively. There is thus no clear preference between the two canonical forms, as the stabilization effect by charge delocalization in the structure on the left is partially offset by the increased electrostatic repulsion between Na^+ and $C1'^+$.

The small energy differences among structures **2a**, **2b**, and **2c** is comparable to the typical computational error of 2–3 kcal/mol and suggests that all three species could be significantly

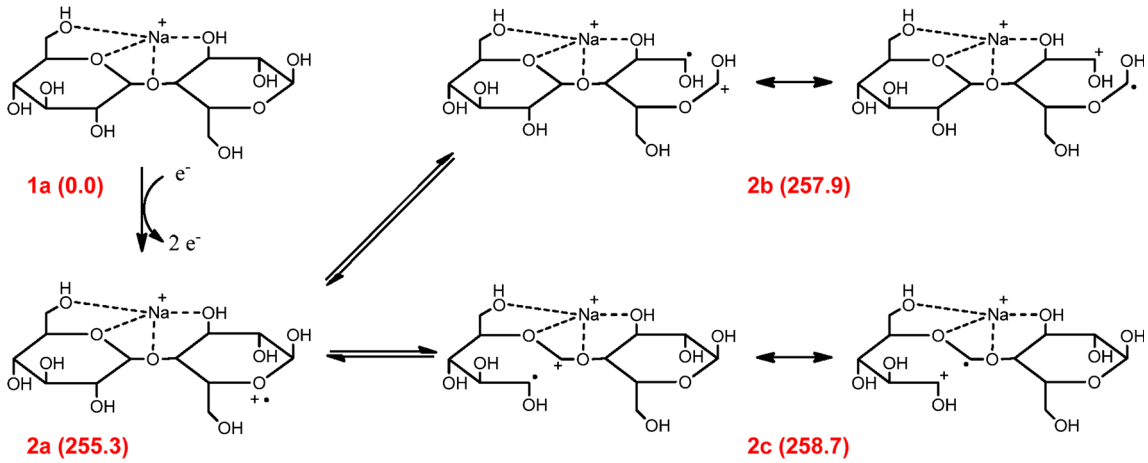

Scheme 1. Ionization of the cellobiose-Na^+ complex. The numbers in parentheses indicate the potential energy (in kcal/mol) of each ionized species relative to **1a**

populated upon ionization, as a difference of 1 kcal/mol in energy between two structures only translates to a 5.4-fold difference in their Boltzmann distribution weights at room temperature. Since the actual internal temperature of the ionized species was likely higher because of the radiative heating from the hot cathode dispenser and, more importantly, because of the excess energy deposit upon irradiation by high-energy electrons, the population difference among these structures might be even smaller.

Formation of Diradicals upon Electron Recapture

In the original EED study, it was proposed that the distonic peptide ion can capture a low-energy electron to form an electronically excited precursor ion, likely in the form of a diradical. Here, electron recapture by the radical cation **2a** would form a closed-shell species, and shut down all radical-driven fragmentation channels. This excited closed-shell species would then undergo CAD-type dissociation, generating primarily glycosidic fragments and small neutral losses.

Meanwhile, electron recapture by the distonic ions **2b** and **2c** should lead to the formation of open-shell diradicals **3a** and **3b**, with their spin density distributions illustrated in Figure 3. The energy releases associated with the electron recapture process are 178 and 188.6 kcal/mol for **2b** and **2c**, respectively. The two radical sites in **3a** are C1 and C2, and those in **3b** are C1′ and C2′. The radical reactivity of a diradical is affected by its singlet-triplet splitting (S-T gap). If the S-T gap is trivial or significantly positive, the coupling between the two radical sites is weak and the diradical behaves as two independent radicals. On the other hand, a large negative S-T gap would indicate a stable open-shell singlet ground state with strong coupling between the two unpaired electrons and the lack of radical reactivity. Therefore, it is essential to estimate the S-T gaps in a mechanistic study that involves diradicals.

Although it is relatively easy to calculate the triplet state energy since a single-reference based quantum mechanics method would suffice, a multi-reference based method, such as CASSCF, CASPT2, or MRCI, is needed for calculation of the open-shell, singlet state energy. As these multi-reference based methods are beyond our computational capability, a specially designed method within the single-reference based DFT frame was utilized here to calculate the S-T gap [31]. Briefly, a 50:50 mixture of the singlet and the triplet states was generated by flipping the spin of the highest energy SOMO of the triplet state, and the S-T gap was estimated to be twice the splitting between the triplet and the 50:50 mixing states. When calculated at the B3LYP/6-31G(d) level, the singlet-triplet splitting was found to be –0.04 kcal/mol for the diradical **3a**, and 0.027 kcal/mol for the diradical **3b**. The trivial S-T gap suggests that there is little interaction between the two unpaired electrons in either diradical and that **3a** and **3b** can undergo typical radical-driven fragmentations. In the following mechanistic study, all calculations were performed on the triplet potential energy surface.

Formation of the Cross-Ring Fragments

The diradical **3a** in its triplet state can undergo radical-induced α-cleavages to form a $^{3,5}A_2$ ion via two pathways, as illustrated in Scheme 2a. The first pathway is initiated by the HCOOH loss, forming a $^{1,5}A_2$ ion which further loses a

Table 2. The Relative Energy (kcal/mol) of the Radical Cation **2a** and the Distonic Ions **2b** and **2c**

	Radical cation 2a	Transition state	Distonic ion 2b	Distonic ion 2c
B3LYP/6-31G(d)	0.0	2.2	2.6	3.4
B3LYP/6-31+G(d,p)//B3LYP/6-31G(d)	0.0	1.4	1.5	3.4
B3LYP/6-311++G(2d,p)//B3LYP/6-31G(d)	0.0	0.5	0.1	2.6
B3LYP/6-311++G(3df,2p)//B3LYP/6-31G(d)	0.0	–0.1	–0.9	1.9

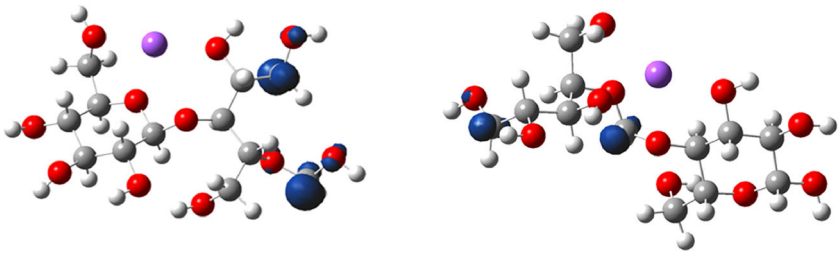

Figure 3. The spin density distributions of the triplet state of the diradicals **3a** and **3b**

dihydroxyethylene molecule to produce the $^{3,5}A_2$ ion. These two reaction steps are exothermic, by 15.5 kcal/mol and 30.9 kcal/mol, respectively. The HCOOH loss is associated with a 7.5 kcal/mol barrier, whereas the dihydroxyethylene loss is barrierless. The second reaction pathway is initiated by the loss of a dihydroxyethylene and the formation of $^{1,3}A_2$ with a 21 kcal/mol endothermicity, followed by the HCOOH loss and the formation of $^{3,5}A_2$, with a 67.4 kcal/mol exothermicity. No tight transition state was found for either reaction step. Similarly, the diradical **3b** can undergo sequential α-cleavages to form a $^{1,5}X_1$ ion via one of the two pathways, as shown in Scheme 2b. The first pathway starts with the cleavage of the O5′–C5′ bond, forming a $^{1,5}X_1$ ion and a neutral diradical. The O5′–C5′ bond cleavage is 21.2 kcal/mol endothermic, and does not have a canonical tight transition state. The neutral diradical then undergoes the C3′–C4′ cleavage to form two closed-shell species. The second dissociation channel involves sequential losses of dihydroxyethylene and dihydroxypropylene, both without a tight transition state. The dihydroxyethylene loss is 27.7 kcal/mol endothermic, and the final product is 12 kcal/mol lower in energy than the diradical **3b**. Because of the large energy deposit into the diradicals **3a** and **3b** (178 and 188.6 kcal/mol, respectively) during the electron recapture step, all reaction channels are energetically accessible. The intermediate product $^{1,5}A_2$ is observed with low abundance in the EED spectrum, but the formation of the $^{1,3}A_2$ and $^{1,3}X_1$ ions cannot be verified as they both result from the loss of a dihydroxyethylene molecule, which can occur via several different pathways and is common in the tandem mass spectra of carbohydrates.

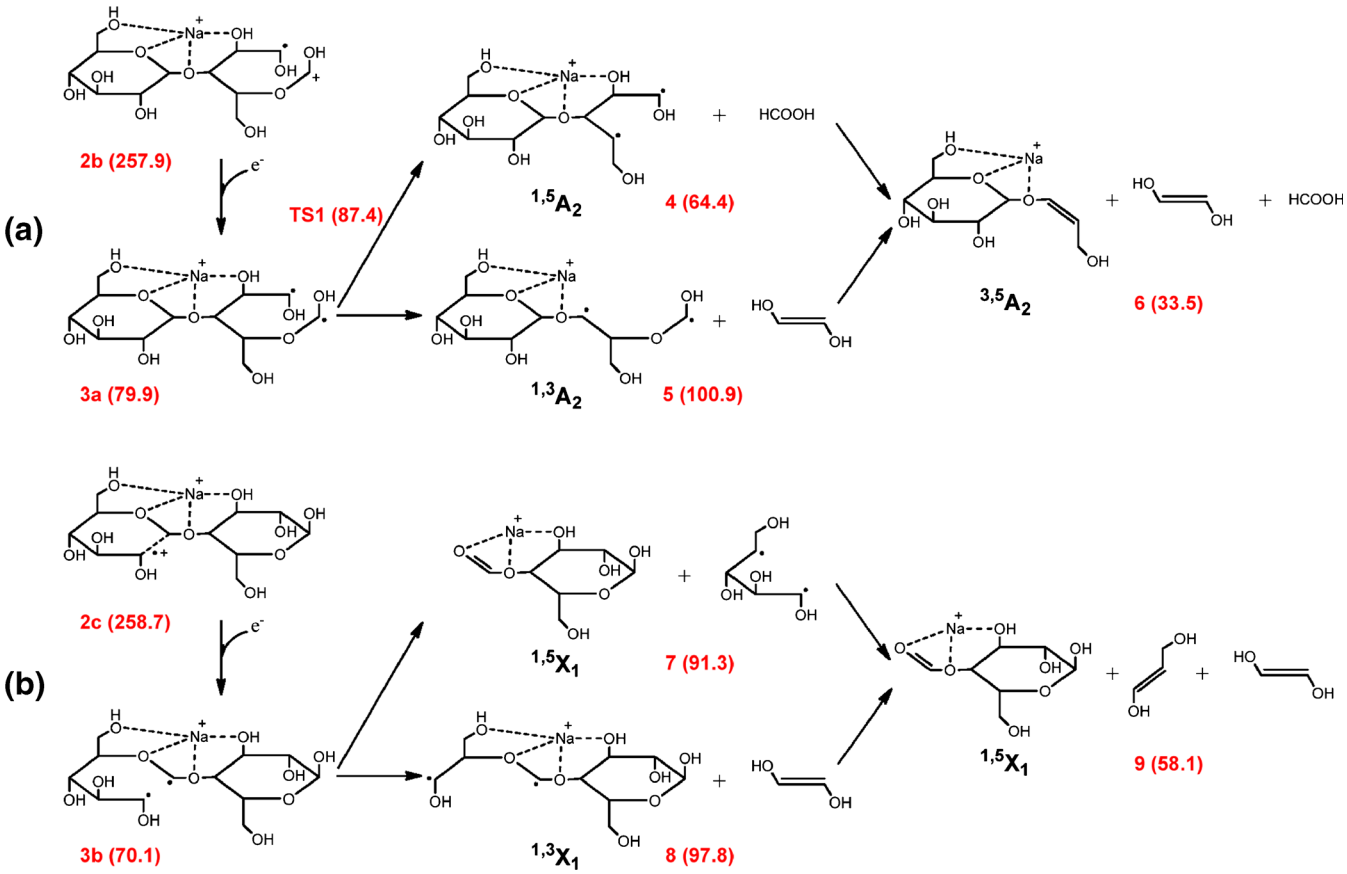

Scheme 2. Proposed mechanism for the formation of (**a**) $^{3,5}A_2$ and (**b**) $^{1,5}X_1$ ions. The numbers in parentheses indicate the zero Kelvin enthalpies (in kcal/mol) of each species relative to structure **1a**

Experimentally, the $^{3,5}A_2$ and $^{1,5}X_1$ ions were the two most abundant cross-ring fragments found in the 12 eV EED spectrum of the cellobiose-Na^+ complex. This observation is consistent with the fact that they are closed-shell products deriving from the two most stable distonic ions, **2b** and **2c**. Formation of the other two major cross-ring fragments, $^{2,4}A_2$ and $^{0,2}X_1$, likely involves different distonic ions, **2d** and **2e**, respectively (Supporting Scheme S2). In contrast to structures **2b** and **2c**, where the positive charge is resonantly stabilized by two oxygen atoms, the positive charge in **2d** and **2e** is stabilized by only one oxygen atom. Structure **2d** is 13.6 kcal/mol higher in energy than the radical cation **2a**, whereas **2e** is 22.5 kcal/mol higher in energy than **2a**. Consequently, cross-ring fragments originated from **2d** and **2e**, the $^{2,4}A_2$ and $^{0,2}X_1$ ions, were present in much lower abundances than $^{3,5}A_2$ and $^{1,5}X_1$. The abundance of the $^{2,4}A_2$ and $^{0,2}X_1$ ions dropped further at lower excitation energies, and these products of higher-energy channels were barely observed as the excitation energy approached the ionization threshold (Supporting Figure S1).

Fragmentation via Direct Electronic Excitation without Ionization

Irradiation by high-energy electrons may also result in direct electronic excitation and dissociation of the cellobiose-Na^+ complex without the ionization-recapture process. The rigorous treatment of the excited states requires the utilization of multi-reference based ab initio methods with extensive basis sets. However, investigation of the excited states of the cellobiose-Na^+ system by multi-reference methods is beyond our current computational capabilities. In this study, TDDFT was applied at the affordable B3LYP/6-31G(d) level to provide a qualitative view of the excitation and dissociation processes.

Since direct excitation of the closed-shell cellobiose-Na^+ complex to a triplet state is spin-forbidden, only dissociation from the singlet excited states is considered here. This may proceed via one of the three possible pathways. First, a singlet excited state may directly dissociate into a closed-shell neutral and a closed-shell cation, without radical intermediates. This channel can be accessed only if two electrons are simultaneously excited, but this is unlikely under the EED condition. Second, a singlet excited state may cross to an energetically adjacent triplet excited state, and subsequently relax to a triplet ground state via conical intersection. Radical driven fragmentation can then occur on the triplet ground state surface. However, the intersystem crossing is insignificant in the cellobiose-Na^+ system as it contains no heavy atoms (such as bromine or iodine) with strong spin-orbital coupling. Lastly, fragmentation can take place from a specific singlet excited state if it can be mainly described by one electronic configuration, formed by excitation of an electron to a specific MO that can be primarily regarded as a localized σ* orbital. If transition to such a singlet excited state has nontrivial oscillator strength, it can result in the homolytic cleavage of a σ bond to generate two radical sites that lead to radical-driven fragmentations.

To evaluate the accessibility of the third channel, we calculated the energetics of the vertical excitation to the first 400 singlet excited states, up to an excitation energy of 11.65 eV, exceeding the ionization threshold. The first 5 singlet excited states can be mainly described by a single configuration, generated by excitation of an electron from the highest occupied molecular orbital (HOMO, MO 96) or other occupied orbitals of 1**a** to its lowest unoccupied molecular orbital (LUMO, MO 97) (Figure 4), with the excitation energy ranging from 5.77 to 6.32 eV. The LUMO of the ground state can be regarded as the 4s Rydberg orbital of Na, characterized by its large coefficient (0.8437) in the LUMO's expression. Such excitations would lead to the neutralization of Na^+ and the loss of a Na atom from the complex, suggesting that low-energy excited states do not contribute significantly to the fragmentation of the cellobiose-Na^+ complex.

Transitions to the next 395 singlet excited states are characterized by very narrow energy spacing between adjacent excitations, even at the relatively small 6-31G(d) basis set level used here. At an excitation energy of 11 eV, the density of states has already reached 154 states per eV. At even higher excitation energies, the state distribution function could become continuous. These transitions all have relatively small oscillating strength, with the largest being 0.04 for the excitation to the 197th state. The computed UV spectrum will be a broad band with low intensity, as the parent ion lacks heavy atoms and π electrons. These higher energy excited states are characterized by multiple configurations, representing the excitation of an electron to the unoccupied MOs 97-129. The population analysis revealed that the main contributors to these MOs are the 2s Rydberg orbital of hydrogen, followed by the 3s Rydberg orbital of oxygen, and the 3s and 3p Rydberg orbitals of carbon. These MOs are generally canonical and more appropriately described as Rydberg orbitals than σ* orbitals. Therefore, at excitation energies below 11.65 eV, direct dissociation from a specific excited state should not be

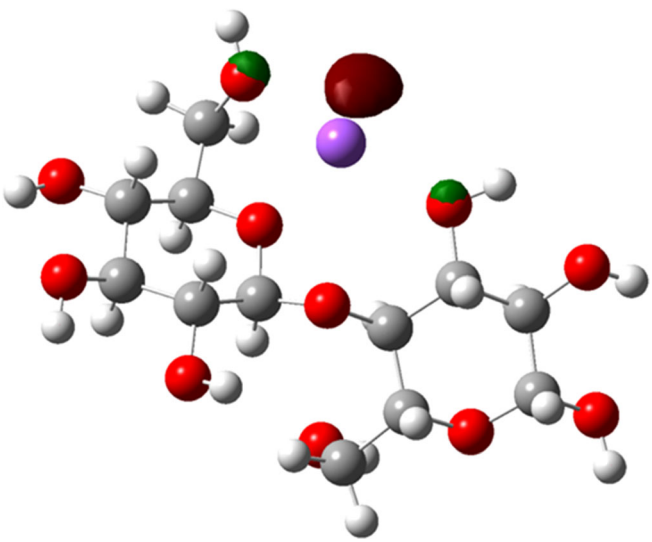

Figure 4. The LUMO of the ground state of the lowest energy conformer of the cellobiose-Na^+ complex

a major channel, even if its occurrence cannot be completely ruled out. Experimentally, the onset for formation of the $^{3,5}A_2$ and $^{1,5}X_1$ ions was observed at a cathode bias of –10 V (Supporting Figure S1), when the energy of electrons at the high-energy tail of the electron population just exceeded the ionization potential of the cellobiose-Na^+ complex, allowing the complex to fragment via the ionization-recapture pathway as proposed above.

Implications of the Ionization-Recapture Mechanism

Unlike in ECD, where the electron is initially captured by the metal cation, the electron recapture in EED occurs at a site remote from the metal charge carrier. As such, glycans adducted with different metal cations often produce similar EED fragmentation patterns, whereas their ECD fragmentation behaviors can differ dramatically because of the different electronic properties of the metal charge carriers. Further, in ECD, radical formation at a specific site is determined by its spatial proximity to the metal cation, and this can result in limited, localized fragmentation. In EED, the metal cation is not directly involved in the ionization-recapture process; thus, the radical can be formed at any of many sites along the glycan sequence, leading to more diverse fragmentation. The proposed EED mechanism also suggests that the electron energy has a profound effect on the accessibility of various fragmentation channels, especially near the ionization threshold, where fragment ions derived from the most stable distonic ions were preferentially produced. After electron recapture, the diradical tends to undergo consecutive α-cleavages until the two radicals recombine to form a closed-shell species. For a hexose residue, cleavage of the C1–C2 bond is favored because of charge delocalization in the resultant distonic ion, leading to predominantly $^{1,5}X$- and $^{3,5}A$-type ions. The nature of the monosaccharide residue, its branching pattern and linkage configuration, as well as the derivatization chemistry, such as permethylation and reductive amination, can all influence the stability of the distonic ion, and consequently, the EED fragmentation patterns. For example, enhanced 2,4-cross-ring cleavages at *N*-acetyl glucosamine (GlcNAc) residues were observed in EED of the doubly sodiated hexaacetylchitohexaose (GlcNAc-β1,4-[GlcNAc-β1,4-]$_4$GlcNAc, Supporting Figure S2).

Conclusions

Using the cellobiose-Na^+ complex as the model system, the fragmentation behavior of metal-bound glycans upon irradiation by electrons with energy exceeding their ionization potential was investigated by FTICR MS and theoretical modeling. It was found that high-energy electron irradiation can lead to ionization of the glycan, generating a mixture of radical cations and various ring-opened distonic ions. Upon recapturing a low-energy electron, these distonic ions formed diradicals with trivial singlet-triplet splitting. The triplet diradicals then underwent radical-driven reactions to produce a variety of fragment ions. Since only fragment ions originating from the most stable distonic ions are abundantly formed near the threshold, EED should be performed at electron energy of several eV above the ionization potential to maximize the structural information content in the resulting tandem mass spectra. Further studies are needed to understand the effect of glycan structural variables, including the presence of various chemical modifications, on the glycan EED fragmentation behavior.

Acknowledgments

The authors gratefully acknowledge the financial support from the National Institutes of Health via research grants P41 GM104603 and S10 RR025082. The authors also acknowledge the technical support and the computing resources provided by the Scientific Computing and Visualization Group at Boston University.

References

1. Cody, R.B., Freiser, B.S.: Electron-impact excitation of ions from organics - alternative to collision-induced dissociation. Anal. Chem. **51**, 547–551 (1979)
2. Zubarev, R.A., Kelleher, N.L., McLafferty, F.W.: Electron capture dissociation of multiply charged protein cations. A nonergodic process. J. Am. Chem. Soc. **120**, 3265–3266 (1998)
3. Syka, J.E., Coon, J.J., Schroeder, M.J., Shabanowitz, J., Hunt, D.F.: Peptide and protein sequence analysis by electron transfer dissociation mass spectrometry. Proc. Natl. Acad. Sci. U. S. A. **101**, 9528–9533 (2004)
4. Cooper, H.J., Håkansson, K., Marshall, A.G.: The role of electron capture dissociation in biomolecular analysis. Mass Spectrom. Rev. **24**, 201–222 (2005)
5. Mikesh, L.M., Ueberheide, B., Chi, A., Coon, J.J., Syka, J.E.P., Shabanowitz, J., Hunt, D.F.: The utility of ETD mass spectrometry in proteomic analysis. Biochim. Biophys. Acta Proteins Proteomics **1764**, 1811–1822 (2006)
6. Witze, E.S., Old, W.M., Resing, K.A., Ahn, N.G.: Mapping protein post-translational modifications with mass spectrometry. Nat. Methods **4**, 798–806 (2007)
7. Kjeldsen, F., Haselmann, K.F., Budnik, B.A., Jensen, F., Zubarev, R.A.: Dissociative capture of hot (3-13 eV) electrons by polypeptide polycations: an efficient process accompanied by secondary fragmentation. Chem. Phys. Lett. **356**, 201–206 (2002)
8. Nielsen, M.L., Budnik, B.A., Haselmann, K.F., Olsen, J.V., Zubarev, R.A.: Intramolecular hydrogen atom transfer in hydrogen-deficient polypeptide radical cations. Chem. Phys. Lett. **330**, 558–562 (2000)
9. Nielsen, M.L., Budnik, B.A., Haselmann, K.F., Zubarev, R.A.: Tandem MALDI/EI ionization for tandem Fourier transform ion cyclotron resonance mass spectrometry of polypeptides. Int. J. Mass Spectrom. **226**, 181–187 (2003)
10. Fung, Y.M.E., Adams, C.M., Zubarev, R.A.: Electron ionization dissociation of singly and multiply charged peptides. J. Am. Chem. Soc. **131**, 9977–9985 (2009)
11. Adamson, J.T., Håkansson, K.: Electron detachment dissociation of neutral and sialylated oligosaccharides. J. Am. Soc. Mass Spectrom. **18**, 2162–2172 (2007)
12. Wolff, J.J., Amster, I.J., Chi, L.L., Linhardt, R.J.: Electron detachment dissociation of glycosaminoglycan tetrasaccharides. J. Am. Soc. Mass Spectrom. **18**, 234–244 (2007)
13. Wolff, J.J., Leach, F.E., Laremore, T.N., Kaplan, D.A., Easterling, M.L., Linhardt, R.J., Amster, I.J.: Negative electron transfer dissociation of glycosaminoglycans. Anal. Chem. **82**, 3460–3466 (2010)
14. Huang, Y., Yu, X., Mao, Y., Costello, C.E., Zaia, J., Lin, C.: De Novo sequencing of heparan sulfate oligosaccharides by electron-activated dissociation. Anal. Chem. **85**, 11979–11986 (2013)

15. Adamson, J.T., Håkansson, K.: Electron capture dissociation of oligosaccharides ionized with alkali, alkaline earth, and transition metals. Anal. Chem. **79**, 2901–2910 (2007)
16. Zhao, C., Xie, B., Chan, S.Y., Costello, C.E., O'Connor, P.B.: Collisionally activated dissociation and electron capture dissociation provide complementary structural information for branched permethylated oligosaccharides. J. Am. Soc. Mass Spectrom. **19**, 138–150 (2008)
17. Han, L., Costello, C.E.: Electron transfer dissociation of milk oligosaccharides. J. Am. Soc. Mass Spectrom. **22**, 997–1013 (2011)
18. Kailemia, M.J., Ruhaak, L.R., Lebrilla, C.B., Amster, I.J.: Oligosaccharide analysis by mass spectrometry: a review of recent developments. Anal. Chem. **86**, 196–212 (2013)
19. Yu, X., Huang, Y., Lin, C., Costello, C.E.: Energy-dependent electron activated dissociation of metal-adducted permethylated oligosaccharides. Anal. Chem. **84**, 7487–7494 (2012)
20. Yu, X., Jiang, Y., Chen, Y., Huang, Y., Costello, C.E., Lin, C.: Detailed glycan structural characterization by electronic excitation dissociation. Anal. Chem. **85**, 10017–10021 (2013)
21. Budnik, B., Haselmann, K., Elkin, Y.N., Gorbach, V., Zubarev, R.: Applications of electron-ion dissociation reactions for analysis of polycationic chitooligosaccharides in Fourier transform mass spectrometry. Anal. Chem. **75**, 5994–6001 (2003)
22. Gao, D., Zhou, W., Håkansson, K.: Electron induced dissociation (EID) of singly protonated glycans. Proceedings of the 58th ASMS Conference on Mass Spectrometry and Allied Topics, Salt Lake City, UT, 23–27 May 2010
23. Wolff, J.J., Laremore, T.N., Aslam, H., Linhardt, R.J., Amster, I.J.: Electron-induced dissociation of glycosaminoglycan tetrasaccharides. J. Am. Soc. Mass Spectrom. **19**, 1449–1458 (2008)
24. Huang, Y., Pu, Y., Yu, X., Costello, C., Lin, C.: Mechanistic study on electron capture dissociation of the oligosaccharide-Mg2+ complex. J. Am. Soc. Mass Spectrom. **25**, 1451–1460 (2014)
25. Scott, A.P., Radom, L.: Harmonic vibrational frequencies: an evaluation of Hartree-Fock, Møller-Plesset, Quadratic Configuration Interaction, Density Functional Theory, and Semiempirical Scale Factors. J. Phys. Chem. **100**, 16502–16513 (1996)
26. Frisch, M.J., Trucks, G.W., Schlegel, H.B., Scuseria, G.E., Robb, M.A., Cheeseman, J.R., Montgomery, J.A.J., Vreven, T., Kudin, K.N., Burant, J.C., Millam, J.M., Iyengar, S.S., Tomasi, J., Barone, V., Mennucci, B., Cossi, M., Scalmani, G., Rega, N., Petersson, G.A., Nakatsuji, H., Hada, M., Ehara, M., Toyota, K., Fukuda, R., Hasegawa, J., Ishida, M., Nakajima, T., Honda, Y., Kitao, O., Nakai, H., Klene, M., Li, X., Knox, J.E., Hratchian, H.P., Cross, J.B., Bakken, V., Adamo, C., Jaramillo, J., Gomperts, R., Stratmann, R.E., Yazyev, O., Austin, A.J., Cammi, R., Pomelli, C., Ochterski, J.W., Ayala, P.Y., Morokuma, K., Voth, G.A., Salvador, P., Dannenberg, J.J., Zakrzewski, V.G., Dapprich, S., Daniels, A.D., Strain, M.C., Farkas, O., Malick, D.K., Rabuck, A.D., Raghavachari, K., Foresman, J.B., Ortiz, J.V., Cui, Q., Baboul, A.G., Clifford, S., Cioslowski, J., Stefanov, B.B., Liu, G., Liashenko, A., Piskorz, P., Komaromi, I., Martin, R.L., Fox, D.J., Keith, T., Al-Laham, M.A., Peng, C.Y., Nanayakkara, A., Challacombe, M., Gill, P.M.W., Johnson, B., Chen, W., Wong, M.W., Gonzalez, C., Pople, J.A.: Gaussian v C.02. Gaussian, Inc., Wallingford (2004)
27. Domon, B., Costello, C.E.: A systematic nomenclature for carbohydrate fragmentations in Fab-Ms MS Spectra of glycoconjugates. Glycoconj. J. **5**, 397–409 (1988)
28. Weimar, T., Kreis, U.C., Andrews, J.S., Pinto, B.M.: Conformational analysis of maltoside heteroanalogues using high-quality NOE data and molecular mechanics calculations. Flexibility as a function of the interglycosidic chalcogen atom. Carbohydr. Res. **315**, 222–233 (1999)
29. Mendonca, S., Johnson, G.P., French, A.D., Laine, R.A.: Conformational analyses of native and permethylated disaccharides. J. Phys. Chem. A **106**, 4115–4124 (2002)
30. da Silva, C.O., Nascimento, M.A.C.: Ab initio conformational maps for disaccharides in gas phase and aqueous solution. Carbohydr. Res. **339**, 113–122 (2004)
31. Cramer, C.J., Dulles, F.J., Giesen, D.J., Almlöf, J.: Density functional theory: excited states and spin annihilation. Chem. Phys. Lett. **245**, 165–170 (1995)